COMPARISON OF SEVERAL N - FACTOR INTEGRATION STRATEGIES IN A COMPRESSIBLE BOUNDARY LAYER OVER A SWEPT CURVED SURFACE

J. C. F. Pereira and J. M. M. Sousa

Instituto Superior Técnico/Technical University of Lisbon
Mechanical Engineering Department
Av. Rovisco Pais
1096 Lisbon Codex
Portugal

Abstract. Several N - factor integration strategies for transition prediction using linear stability analysis are compared. A three-dimensional compressible formulation of the problem, taking into account the curvature effects but under the assumption of parallel flow, was used in conjunction with experimental information regarding the occurrence of transition. This procedure allowed to establish more consistent correlations for predicting the transition location in the flow over a swept wing, employing the e^N - method. The present results have demonstrated that the effects of surface curvature are predominant when compared with those due to streamline curvature, inducing a strong stabilizing influence on the crossflow - dominated cases that have been investigated.

Introduction

The e^N - method is still the current state-of-the-art procedure for predicting the onset of transition in both incompressible and compressible flows. Its fundamentals[1],[2] are well known and the method is characterized by the coupling of a theoretical basis (linear stability theory) and the empiricism associated to the N - factor itself, which is computed by integrating "small" disturbance amplification rates yielded by the aforementioned theory. Here, "small" means that quadratic terms in the disturbance amplitudes may be neglected in comparison with linear terms. The success in the use of the e^N - method is strongly correlated to an efficient calibration of the N - factor value at the transition location for the flow under analysis. Although for two - dimensional flows a quasi-universal value has been established, it has not been possible to do it, with the same generality, for example for three - dimensional flows. Moreover, while it is recognized that there are several effects which influence the transition process and, consequently, its onset, such as the pressure gradient, the Mach number (compressibility), the wall temperature, the surface roughness, mass transfer and both streamline and surface curvatures, most of previous studies on the present subject have only accounted for a few of these effects, further limiting the accuracy of the analysis.

The recently increased interest in the e^N - method has been brought about mainly by its application as an indispensable design tool in the framework of

laminar flow control techniques to be implemented in commercial aircraft. However, as the flow under consideration is three - dimensional (boundary layers over swept wings[3]-[6]), the integration procedure is less straight - forward than the corresponding one in two - dimensional flows, due to the new possible integration strategies to evaluate the N - factor, as pointed out by Malik and Orszag.[7] Investigations performed without taking into account curvature effects[4] have reported N - factor values at transition ranging from 1 to 20, which introduces many drawbacks for the establishment of the e^N - method as a reliable tool for transition prediction. In order to extend the applicability of this method, a few researchers have already included the effects of streamline and surface curvature in their analyses.[8]-[13] The general consensus points that the accuracy of the method is usually improved since, for instance, convex surface curvature has proved to produce a significant stabilizing influence on the laminar boundary layer.

The objective of the present paper is to compare the performance of various N - factor integration strategies, such as the envelope method, fixed frequency/fixed wavelength and fixed frequency/fixed orientation, emphasizing and exploiting the effects of surface and streamline curvatures on the computed N - factor value, for three - dimensional boundary layers over a realistic swept curved surface. Information about transition locations was available which allowed to postulate the "best" strategies. In the next section, the equations ruling the behavior of "small" disturbances in a compressible three - dimensional boundary layer, formulated in an orthogonal curvilinear coordinate system, are presented. Aiming to solve the resulting set of equations, they have been embedded into the COSALX algorithm.[14] Next, the results obtained using the above mentioned N - factor integration strategies are carefully described. The last section summarizes the main conclusions of this investigation.

Problem Formulation and Numerical Method

Figure 1 depicts the case of three-dimensional flow over a curved swept surface. The figure also shows schematically the geometry and notation for the body-fitted orthogonal curvilinear coordinate system used.

In the present study the basic flow has been obtained from the solution of the compressible boundary layer equations for a perfect gas. The method proposed by Kaups and Cebeci[15] has been employed, thus assuming the invariance of the pressure and velocity fields in the z - direction, i.e., the conical flow assumption was applied.

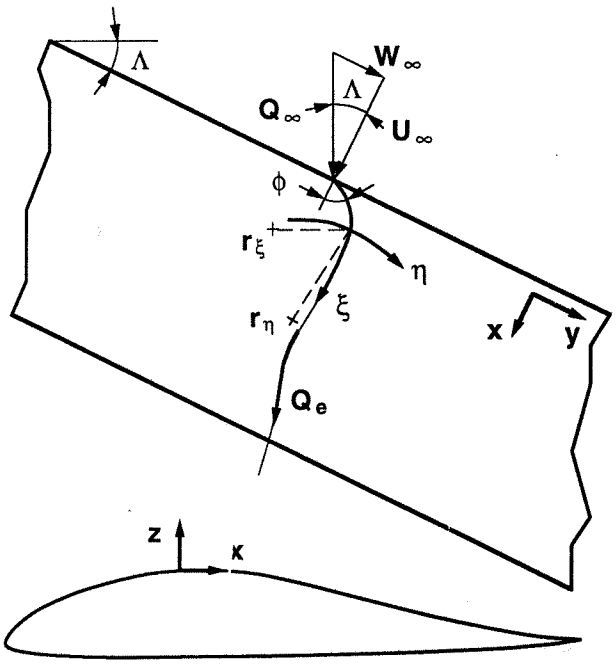

Fig. 1 Flow geometry and notation.

Disturbance Equations

For the formulation of the problem of linear stability analysis, we begin by considering a flow where the instantaneous values of velocity, pressure and temperature may be considered as a superimposition of "infinitesimally small" disturbances on the above mentioned basic state. So, the instantaneous values may be written as

$$(u, v, w, p, T) = (\bar{u}, \bar{v}, \bar{w}, \bar{p}, \bar{T}) + (u', v', w', p', T'), \quad (1)$$

where u, v and w are the orthogonal velocity components, p is the pressure and T stands for the temperature. We further assume the basic flow as quasi - parallel, so that

$$\bar{u} = \bar{u}(z), \quad \bar{v} = 0, \quad \bar{w} = \bar{w}(z), \quad \bar{T} = \bar{T}(z), \quad (2)$$

expressing an approximation which introduces a small error as long as the Reynolds number is high.[11] Here, all the quantities are non-dimensionalized by their corresponding values at the edge of the boundary layer and the compressible definition of the boundary layer displacement thickness in the streamwise direction, δ^*, is used as length scale. The "small" disturbance components may be described by harmonic fluctuations of the form

$$(u', v', w', p', T') = \mathbf{Re}\left[(\hat{u}, \hat{v}, \hat{w}, \hat{p}, \hat{T})(z) \cdot \exp i(\alpha\xi + \beta\eta - \omega t)\right], \quad (3)$$

where α and β are dimensionless real wavenumbers in ξ and η directions, respectively, and $\omega = \omega_r + i\omega_i$ is a dimensionless complex frequency. Therefore, the disturbances are allowed to propagate in space along the direction defined by $\psi = tg^{-1}(\beta/\alpha)$, at constant amplitude, and in time with varying amplitude at a rate ω_i, for a frequency ω_r. After substituting the expressions given above into the Navier - Stokes equations, subtracting out the basic flow terms, linearizing with respect to "small" perturbations and neglecting terms of $\mathbf{O}(Re^{-2})$, the equations governing the disturbance behavior are written as

$$\hat{\rho} = \gamma M_e^2 \frac{\hat{p}}{\bar{T}} - \frac{\hat{T}}{\bar{T}^2} \quad (4)$$

$$(m_{21} + i\alpha)\hat{u} + (m_{12} + i\beta)\hat{v} + \left(m_{13} + m_{23} - \frac{1}{\bar{T}}\frac{d\bar{T}}{dz}\right)\hat{w} + \frac{d\hat{w}}{dz} + \left[m_{21}\bar{u} + m_{12}\bar{v} + i(\alpha\bar{u} + \beta\bar{v} - \omega)\right]\left(\gamma M_e^2\hat{p} - \frac{\hat{T}}{\bar{T}}\right) = 0 \quad (5)$$

$$\frac{1}{\bar{T}}\left[i(\alpha\bar{u} + \beta\bar{v} - \omega)\hat{u} + \hat{w}\frac{d\bar{u}}{dz} + (\overline{\hat{u}\hat{v}} + \overline{\hat{u}\hat{v}})m_{12} + \overline{\hat{u}\hat{w}}m_{13} - 2\overline{\hat{v}\hat{v}}m_{21}\right] + \left(\gamma M_e^2\frac{\hat{p}}{\bar{T}} - \frac{\hat{T}}{\bar{T}^2}\right)(\overline{\hat{u}\hat{v}}m_{12} - \bar{v}^2 m_{21}) = -i\alpha\hat{p} + \frac{\bar{\mu}}{Re}\left\{\frac{d^2\hat{u}}{dz^2} + \left(1 + \frac{\bar{\lambda}}{\bar{\mu}}\right)\left(i\alpha\frac{d\hat{w}}{dz} - \alpha\beta\hat{v}\right) - \left(2 + \frac{\bar{\lambda}}{\bar{\mu}}\right)\alpha^2\hat{u} - \beta^2\hat{u} + \frac{1}{\bar{\mu}}\frac{d\bar{\mu}}{d\bar{T}}\left[\left(\frac{d\hat{u}}{dz} + i\alpha\hat{w}\right)\frac{d\bar{T}}{dz} + \frac{d\bar{u}}{dz}\frac{d\hat{T}}{dz} + \frac{d^2\bar{u}}{dz^2}\hat{T}\right] + \frac{1}{\bar{\mu}}\frac{d^2\bar{\mu}}{d\bar{T}^2}\frac{d\bar{T}}{dz}\hat{T}\frac{d\bar{u}}{dz}\right\} \quad (6)$$

$$\frac{1}{\bar{T}}\left[i(\alpha\bar{u} + \beta\bar{v} - \omega)\hat{v} + \hat{w}\frac{d\bar{v}}{dz} + (\overline{\hat{v}\hat{u}} + \overline{\hat{v}\hat{u}})m_{21} + \overline{\hat{v}\hat{w}}m_{23} - 2\overline{\hat{u}\hat{u}}m_{12}\right] + \left(\gamma M_e^2\frac{\hat{p}}{\bar{T}} - \frac{\hat{T}}{\bar{T}^2}\right)(\overline{\hat{v}\hat{u}}m_{21} - \bar{u}^2 m_{12}) = -i\beta\hat{p} + \frac{\bar{\mu}}{Re}\left\{\frac{d^2\hat{v}}{dz^2} + \left(1 + \frac{\bar{\lambda}}{\bar{\mu}}\right)\left(i\beta\frac{d\hat{w}}{dz} - \alpha\beta\hat{u}\right) - \left(2 + \frac{\bar{\lambda}}{\bar{\mu}}\right)\beta^2\hat{v} - \alpha^2\hat{v} + \frac{1}{\bar{\mu}}\frac{d\bar{\mu}}{d\bar{T}}\left[\left(\frac{d\hat{v}}{dz} + i\beta\hat{w}\right)\frac{d\bar{T}}{dz} + \frac{d\bar{v}}{dz}\frac{d\hat{T}}{dz} + \frac{d^2\bar{v}}{dz^2}\hat{T}\right] + \frac{1}{\bar{\mu}}\frac{d^2\bar{\mu}}{d\bar{T}^2}\frac{d\bar{T}}{dz}\hat{T}\frac{d\bar{v}}{dz}\right\} \quad (7)$$

$$\frac{1}{\bar{T}}\left[i(\alpha\bar{u}+\beta\bar{v}-\omega)\hat{w}+2\bar{u}\hat{u}m_{13}-2\bar{v}\hat{v}m_{23}\right]-$$
$$\left(\gamma M_e^2\frac{\hat{p}}{\bar{T}}-\frac{\hat{T}}{\bar{T}^2}\right)(\bar{u}^2m_{13}+\bar{v}^2m_{23})=-\frac{d\hat{p}}{dz}+$$
$$\frac{\bar{\mu}}{Re}\left\{\left(2+\frac{\bar{\lambda}}{\bar{\mu}}\right)\frac{d^2\hat{w}}{dz^2}+\left(1+\frac{\bar{\lambda}}{\bar{\mu}}\right)\left(i\alpha\frac{d\hat{u}}{dz}+i\beta\frac{d\hat{v}}{dz}\right)-\right. \qquad (8)$$
$$(\alpha^2+\beta^2)\hat{w}+\frac{1}{\bar{\mu}}\frac{d\bar{\mu}}{d\bar{T}}\left[\left(2+\frac{\bar{\lambda}}{\bar{\mu}}\right)\frac{d\bar{T}}{dz}\frac{d\hat{w}}{dz}+\right.$$
$$\left.\left.i\alpha\frac{d\bar{u}}{dz}\hat{T}+i\beta\frac{d\bar{v}}{dz}\hat{T}+\frac{\bar{\lambda}}{\bar{\mu}}\frac{d\bar{T}}{dz}(i\alpha\hat{u}+i\beta\hat{v})\right]\right\}$$

$$\frac{1}{\bar{T}}\left[i(\alpha\bar{u}+\beta\bar{v}-\omega)\hat{T}+\hat{w}\frac{d\bar{T}}{dz}\right]-$$
$$(\gamma-1)M_e^2\left[i(\alpha\bar{u}+\beta\bar{v}-\omega)\hat{p}\right]=$$
$$\frac{\bar{\mu}}{Pr\,Re}\left[-(\alpha^2+\beta^2)\hat{T}+\frac{d^2\hat{T}}{dz^2}+\frac{1}{\bar{\mu}}\frac{d\bar{\mu}}{d\bar{T}}\left(\hat{T}\frac{d^2\bar{T}}{dz^2}+\right.\right.$$
$$\left.2\frac{d\bar{T}}{dz}\frac{d\hat{T}}{dz}\right)+\frac{1}{\bar{\mu}}\frac{d^2\bar{\mu}}{d\bar{T}^2}\left(\frac{d\bar{T}}{dz}\right)^2\hat{T}\left.\right]+ \qquad (9)$$
$$\frac{(\gamma-1)M_e^2}{Re}\bar{\mu}\left\{2\left(\frac{d\hat{u}}{dz}+i\alpha\hat{w}\right)\frac{d\bar{u}}{dz}+\right.$$
$$\left.2\left(\frac{d\hat{v}}{dz}+i\beta\hat{w}\right)\frac{d\bar{v}}{dz}+\frac{1}{\bar{\mu}}\frac{d\bar{\mu}}{d\bar{T}}\hat{T}\left[\left(\frac{d\bar{u}}{dz}\right)^2+\left(\frac{d\bar{v}}{dz}\right)^2\right]\right\}$$

The boundary conditions to apply require that the disturbance amplitudes ($\hat{u}$, $\hat{v}$, $\hat{w}$, $\hat{p}$, $\hat{T}$) decay to zero at the wall surface and when approaching the edge of the boundary layer. In the above disturbance equations, Re, Pr and M_e denote, respectively, the Reynolds, Prandtl and local Mach numbers. Further, ρ, μ and γ are properties of the fluid, standing for density, viscosity and adiabatic coefficients, respectively. The terms of $\mathbf{0}(Re^{-2})$ have shown to produce only a mild influence in the final results (less than 1% variations), for the present study. This has been thoroughly investigated by comparisons with calculations in which these terms were retained. Collier and Malik[9] have reported similar findings and the equations derived in their work agree well with Eqs. (4) - (9) presented here.

Curvature Terms

The m_{ij} coefficients appearing in Eq. (5) and in the set of Eqs. (6) - (8) denote the curvature terms. These terms allow to account for the curvature effects in the subsequent linear stability analysis based on Eqs. (4) - (9) coupled with the appropriate boundary conditions. The coefficients m_{12} and m_{21} are flow - dependent and they represent the tangential curvature of the coordinate lines. On the other hand, the coefficients m_{13} and m_{23} express the surface curvature of the body. In order to formulate the expressions for the curvature terms, we shall consider the ξ - lines in Fig. 1 as the external streamlines, additionally introducing the η - lines as being perpendicular to the former ones everywhere. Accordingly, we define

$$m_{12}=\delta^*k_\xi=\frac{\delta^*}{r_\xi}\approx-\delta^*\frac{d\phi}{dx}\cos\phi\,, \qquad (10)$$

$$m_{21}=\delta^*k_\eta=\frac{\delta^*}{r_\eta}\approx-\delta^*\frac{d\phi}{dx}\sin\phi\,. \qquad (11)$$

Thus, we are assuming that the wave fronts of crossflow waves ($\psi = 90^o$) display the same local curvature as the inviscid streamlines. The above formulation is consistent as long as the propagation direction remains close to 90^o. Concerning the surface curvatures, these are obtained from the principal normal curvatures defining the curved contour of the profile shown in Fig. 1, k_x and k_y. These values may be calculated in the frame of the conical coordinates considered in the method of Kaups and Cebeci.[15] Then, as the second normal curvature is taken to be zero for the present problem, the dimensionless curvature terms may be obtained in the rotated coordinate system as

$$m_{13} = \dot{\delta} k_x \cos^2 \phi \ , \qquad (12)$$

$$m_{23} = \dot{\delta} k_x \sin^2 \phi \ . \qquad (13)$$

Method of Solution

The method adopted for solving the linear stability equations was an existing compressible stability analysis computer code known as COSALX,[14] an updated version of COSAL.[16] This procedure proved to be adequate as only minor changes to the original algorithm were required in order to perform the calculations described herein. It should still be mentioned that the code includes both global and local procedures for solving the resulting temporal eigenvalue problem. The local search for the eigenvalue ω is performed by inverting a block - tridiagonal system of equations, using a fully pivoted LU factorization, as the stability equations are discretized by means of a matrix finite - differences method. Once the amplification rate ω_i is computed, an N - factor for transition correlation purposes may be defined as

$$N = \int_{s_o}^{s_t} \frac{\omega_i}{|Re(V_g)|} ds \ , \qquad (14)$$

where the integration path s is the arc length on the body surface along the curve that is everywhere tangent to the direction defined by the real part of the group - velocity vector, $Re\,(V_g) = Re\,(\partial\omega/\partial\alpha,\ \partial\omega/\partial\beta)$.

The N - factor defined by (14) may be obtained following several different strategies for the integration procedure. However, it is rather unphysical to integrate the amplification rates corresponding to disturbances for which the frequency changes along the integration path. For this reason, the three N - factor integration strategies considered here impose that the disturbances must be always periodic in time. The procedure for each strategy is described in the next paragraphs.

Maximum amplification rate. The method searches for the most amplified mode with constant frequency at each boundary layer station. Initial values for the wave orientation and wavelength must be prescribed so that an unstable mode ($\omega_i > 0$) may be found at the starting station. In this case, a process for the estimation of an (α, β) pair corresponding to a disturbance exhibiting the maximum amplification rate and the desired frequency begins. The optimization is performed based on the computed group - velocity vectors. When the optimization loop is completed, the amplification rate is integrated to obtain the associated N - factor.

Fixed frequency/fixed wavelength. A disturbance of constant wavelength and frequency is followed downstream. Given a value for the wavelength and for the initial wave orientation, the method searches for an unstable mode at the starting station. Once that an unstable mode has been found, the code iterates (by changing the wave orientation) until the desired frequency is attained. If one mode exhibiting the imposed frequency and wavelength can be found, it is followed downstream and the N - factor is computed.

Fixed frequency/fixed orientation. A disturbance with specified frequency and orientation is followed downstream. The method searches for an unstable mode at the starting station, based on the prescribed frequency and initial wavelength. When an adequate unstable mode is found, the iteration

procedure to adjust the frequency of the disturbance begins (allowing the wavelength to change). If convergence is achieved, the integral (14) is evaluated and the process continues at next station, using the previously computed value of the wavelength to start with.

Results

To investigate the performance of the various N - factor integration strategies, including the effects of curvature, the flow around the HQ26/14.82 wing section[17] is considered. The problem formulation also accounts for the three-dimensionality and compressibility of the flow. However, the selected test cases are weekly compressible, but strong crossflow is present due to large sweep angles. The main reason why we have chosen the above mentioned geometry was the fact that the profile displays high curvature in the upper side, while in the lower side the curvature is low, as sketched in Fig. 1. Therefore, it seemed the perfect scenario to test a procedure which includes curvature effects in the analysis. Three distinct flow conditions were studied: two of these corresponding to flow over the upper side and one to flow over the lower side. The relevant parameters are indicated in Tab. 1, where Λ_{eff}, Re_c, M_∞ and α denote, respectively, the effective sweep angle, the chord based Reynolds number, the Mach number of the undisturbed flow and the angle of attack of the profile.

Table 1 Description of the test cases.

Rec.	Side	Λ_{eff} (°)	Re_c	M_∞	α (°)
VN223	UPPER	44.93	4.02 E6	0.20	0.02
VN464	UPPER	45.00	4.48 E6	0.23	0.52
VN638	LOWER	44.30	4.40 E6	0.23	6.59

As mentioned in the previous section, the basic flow was computed using the Kaups - Cebeci method, from the measured pressure - coefficient distributions for each of the described flow conditions.

The linear stability analysis was conducted for stationary disturbances as these have been identified to play the dominant role in the transition process for the test cases under consideration.[17] In order to assess the possible improvements obtained by taking into account the effects of curvature, N - factors have been computed following the three strategies described in the previous section, for three situations: without any curvature terms; with surface curvature terms only; and with both surface and streamline curvature terms. These correspond to the three curves displayed in each plot presented later in this paper. As the transition locations were also available[17] through an infrared imaging technique, it was possible to establish a correlation for the N - factor value at the transition location. The aim of this procedure was to determine a strategy for the evaluation of N - factors yielding an approximately constant value for the occurrence of transition under different flow conditions.

The results obtained using the *maximum amplification rate* strategy (the so - called *envelope method*) are shown in Figs. 2, 3 and 4, for the records VN223, VN464 and VN638, respectively. As expected, this strategy produced the largest values of the N - factors, independently of taking into account the curvature effects. Reporting to the N - factors at transition location for each case, it can be seen that clearly larger values are obtained for the upper side cases, about 10 - 11, while a value of about 6 was computed for the lower side case. The inclusion of surface curvature terms in

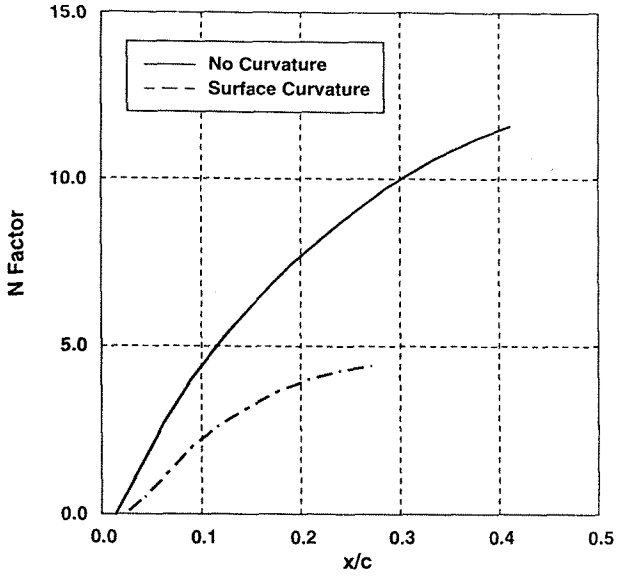

Fig. 2 Evolution of N - factors for VN223, calculated using the envelope method.

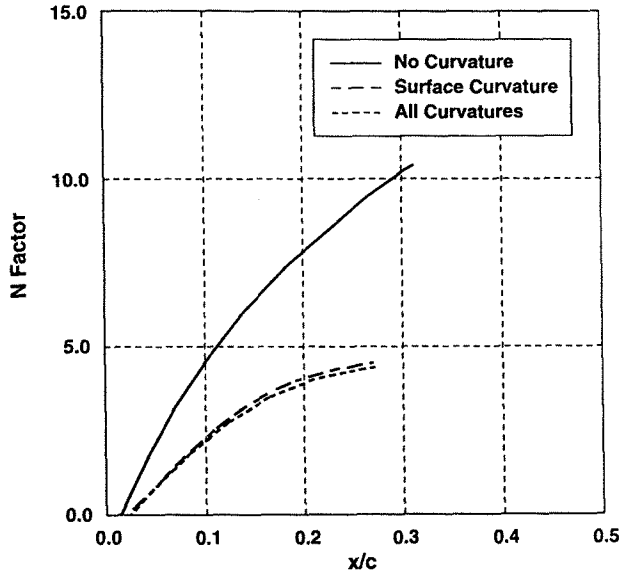

Fig. 3 Evolution of N - factors for VN464, calculated using the envelope method.

the analysis has strongly reduced the N - factors, but a smaller value was still obtained for the lower side flow. Similar results were found when the streamline curvature terms were also included. However, for the record VN223, the stabilizing effect was so strong that no significant N - factor could be computed at the transition location. The summary of these calculations is shown in Tab. 2.

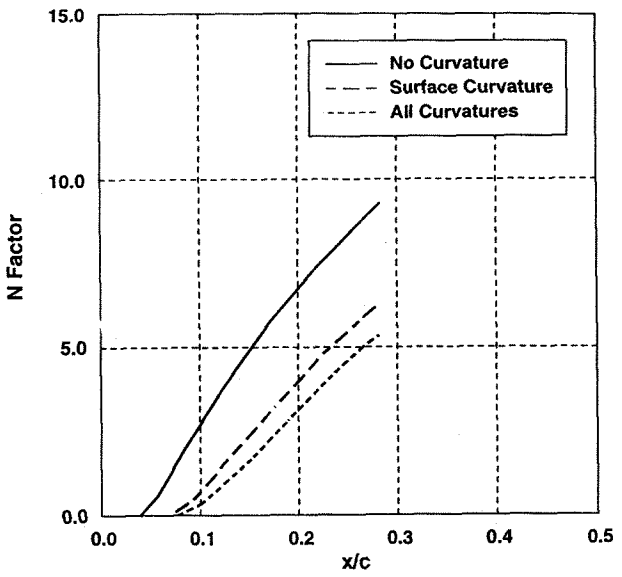

Fig. 4 Evolution of N - factors for VN638, calculated using the envelope method.

In this table the values between parenthesis indicate the location (in percentage of chord) of the stable region that has been encountered (if it was the case) before reaching the experimental transition point at 34%, 27% and 19% of chord for VN223, VN464 and VN638, respectively.

Table 2 N - factors at transition location computed using the maximum amplification rate strategy

Rec.	No Curv	Surf Curv	All Curv
VN223	10.65	4.43 (27.0)	---
VN464	9.59	4.44 (26.8)	4.30 (26.8)
VN638	6.38	3.70	2.85

The evolution of the N - factors computed following the *fixed frequency/fixed wavelength* strategy is shown in Figs. 5,6 and 7, for the records VN223, VN464 and VN638, respectively. Each of the presented curves corresponds, in fact, to an envelope of five curves covering the range of wavelengths (non - dimensionalized by the profile chord) of 0.0020 to 0.0036 for the upper side records and of 0.0024 to 0.0040 for the lower side one. The computed values for the N - factor at

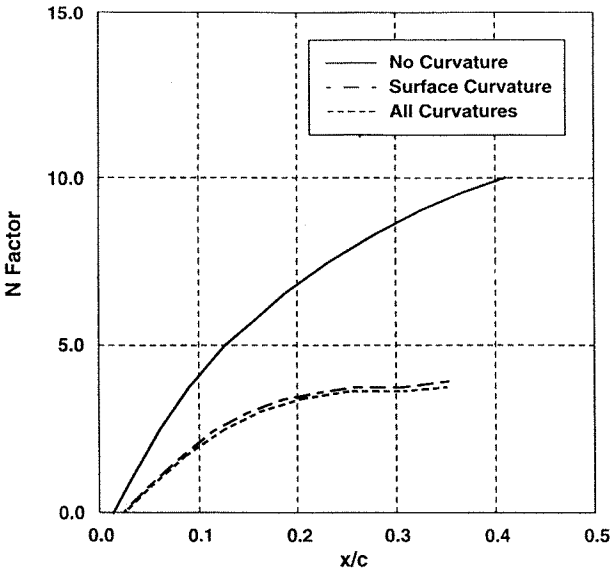

Fig. 5 Evolution of N - factors for VN223, calculated using the fixed frequency and fixed wavelength strategy.

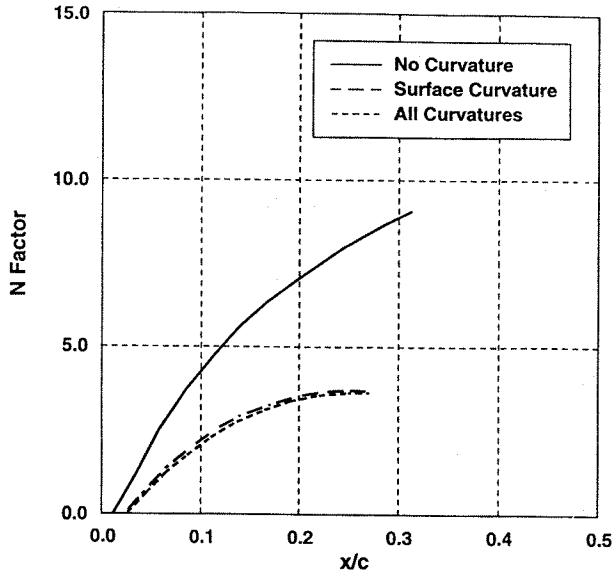

Fig. 6 Evolution of N - factors for VN464, calculated using the fixed frequency and fixed wavelength strategy.

transition location using the present strategy are summarized in Tab. 3. Once again, if the curvature effects are not considered, there is a large difference between the values corresponding to the upper side cases, ranging from 8 to 9, and the value obtained for the lower side case, about 6. These values are in perfect agreement with the

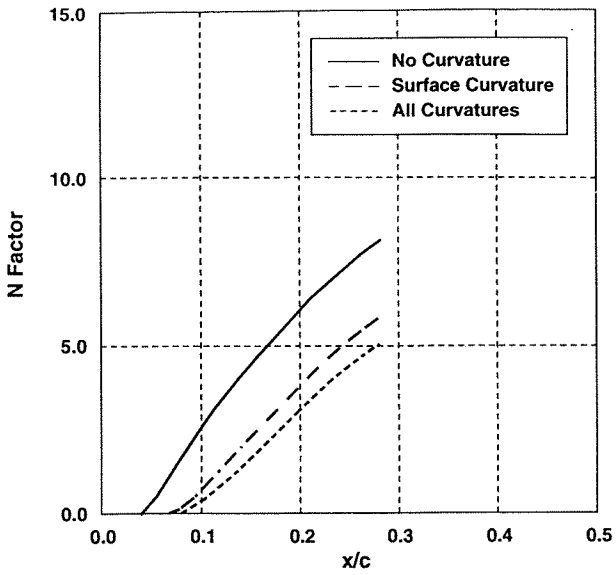

Fig. 7 Evolution of N - factors for VN638, calculated using the fixed frequency and fixed wavelength strategy.

computations of Seitz[17] (also shown in Tab. 3) as expected. However, including the surface curvature terms in the analysis produces an almost constant value for the N - factor at transition location, varying only from 3.5 to 3.8. If the computations are performed with all curvature effects , the results are somehow inconclusive, but it remains clear that the effect of streamline curvature is much less significant (only 3% to 25% of total reduction) than that associated to the geometric curvature of the profile.

Table 3 N - factors at transition location computed using the fixed frequency and fixed wavelength strategy

Rec.	No Curv	Surf Curv	All Curv	(17)
VN223	9.24	3.81	3.67	9.03
VN464	8.36	3.64 (26.8)	3.54 (26.8)	8.33
VN638	5.77	3.47	2.71	5.81

Finally, the results of the N - factor evaluation along the profile employing the *fixed frequency/fixed orientation strategy* are portrayed in Figs. 8, 9 and 10. Again, each curve corresponds to the

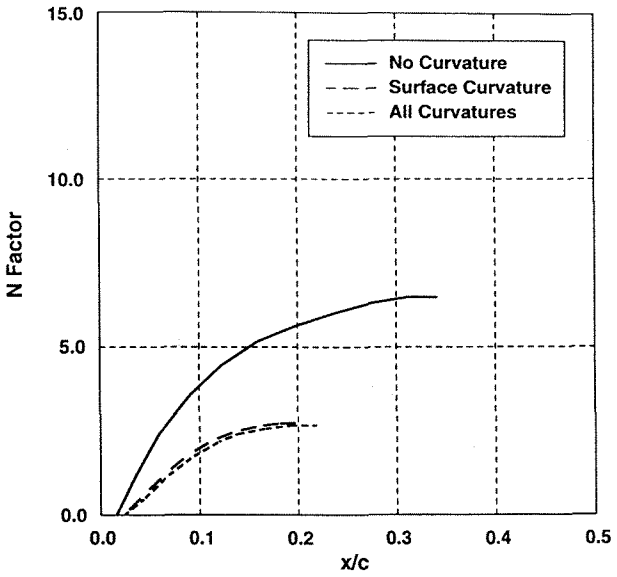

Fig. 8 Evolution of N - factors for VN223, calculated using the fixed frequency and fixed orientation strategy.

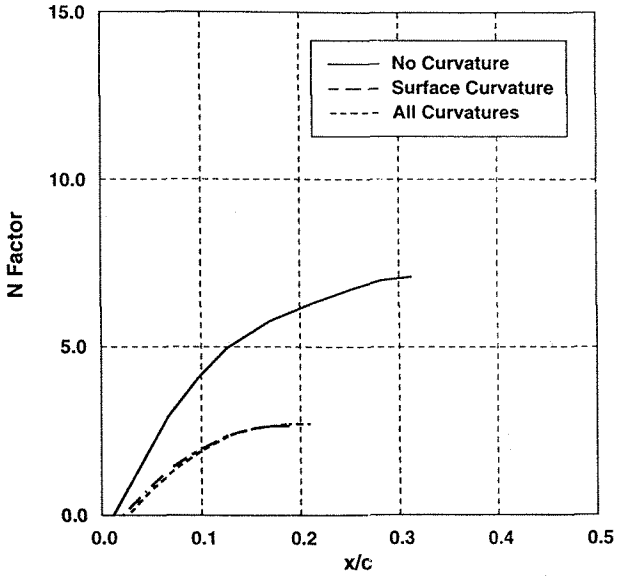

Fig. 9 Evolution of N - factors for VN464, calculated using the fixed frequency and fixed orientation strategy.

envelope curve of five analyzed disturbances, characterized by different orientations. Propagation directions close to pure crossflow direction were selected, ranging from 85° to 87° for VN223 and VN464, but only from 86° to 87° in the case of VN638, which seemed to display a narrower band of amplified disturbances. With

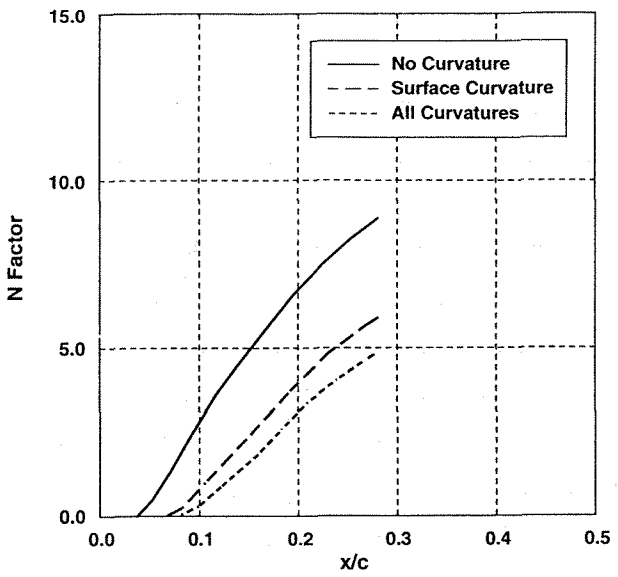

Fig. 10 Evolution of N - factors for VN638, calculated using the fixed frequency and fixed orientation strategy.

regard to the N - factor values at transition location, presented in Tab. 4, we can see that, in contradistinction to the former strategies, the present N - factor integration strategy yields values which are approximately constant, varying from 6.3 to 6.8, even without taking into account any curvature effects. The inclusion of surface curvature terms in the analysis led to inconclusive results, although the general trend of strong stabilization has been, once again, verified. Nevertheless, if we deem to consider all the curvature effects, a constant N - factor value is obtained at the transition location, by following disturbances with fixed orientation, $N_{tr} \approx 2.7$.

Table 4 N - factors at transition location computed using the fixed frequency and fixed orientation strategy

Rec.	No Curv	Surf Curv	All Curv
VN223	6.43 (33.8)	2.64 (19.4)	2.64 (21.8)
VN464	6.84	2.60 (18.6)	2.62 (20.6)
VN638	6.33	3.63	2.72

Conclusions

The effects of curvature on the stability of three-dimensional compressible boundary layers over swept curved surfaces, using several N - factor integration strategies, have been studied. The employed strategies were: maximum amplification rate, fixed wavelength and fixed orientation of disturbances also characterized by a fixed frequency. For the stated purpose, the stability equations governing the amplification of "small" disturbances were implemented in the COSALX algorithm. The integrated N - factors were correlated with the transition location, as this data was available from reported experiments. The inclusion of curvature terms has proved to produce strong stabilizing effects, independently of the integration strategy that has been selected. As a consequence, the computed N - factors at the transition location were quite small and the question arises whether this strong stabilization of the flow is physically realistic or not.

The strategy which follows disturbances with constant frequency and wavelength indicated an approximately constant N - factor value for transition, about 3.6, when the surface curvature effects were considered. For disturbances with fixed frequency and orientation, an excellent correlation for transition was obtained, with $N \simeq 2.7$, particularly when all the curvature effects were taken into account. Even for the maximum amplification rate strategy, the inclusion of curvature effects has proved to constitute a significant improvement if one aims to establish an universal correlation for transition prediction based on the e^N - method.

Acknowledgments

The authors gratefully acknowledge to A. C. de Bruin from NLR for several helpful discussions concerning the COSALX method. We are also indebted to A. Seitz from DLR for providing the information about transition locations and the data to generate the boundary layer profiles from the HQ26 experiments. Part of the present work has been performed in the framework of the ELFIN Project, Brite/Euram Contract no. AERO 1004, and for this reason the authors would like to thank also to B. Dziomba (coordinator) and to H. - W. Stock (task manager).

References

1. Van Ingen, J.L., "A Suggested Semi-Empirical Method for the Calculation of the Boundary Layer Transition Region", Report no.VTH - 74, Delft, The Netherlands, 1956.

2. Smith, A.M.O. and Gamberoni, N., "Transition, Pressure Gradient and Stability Theory", Report no.ES - 26388, Douglas Aircraft Co., El Segundo, California, 1956.

3. Lekoudis, S.G., "Stability of the Boundary Layer on a Swept Wing with Wall Cooling", AIAA J., *18*, 9, 1980, pp 1029 - 1035.

4. Mack, L.M., "Compressible Boundary Layer Stability Calculations for Sweptback Wings with Suction", AIAA J., *20*, 3, 1982, pp 363 - 369.

5. Reed, H.L., "Wave Interactions in Swept Wing Flows", Phys. Fluids, *30*, 11, 1987, pp 3419 - 3425.

6. Casalis, G. and Arnal, D., "Prediction of Transition on a Swept Wing", Rech. Aérosp., *1*, 1990, pp 13 - 22.

7. Malik, M.R. and Orszag, S.A., "Comparison of Methods for Prediction of Transition by Stability Analysis", AIAA J., *18*, 12, 1980, pp 1485 - 1489.

8. Malik, M.R., "Effect of Curvature on Three-Dimensional Boundary Layer Stability", AIAA J., *23*, 9, 1985, pp 1362 - 1369.

9. Collier, F.S. and Malik, M.R., "Curvature Effects on The Stability of Three- Dimensional Laminar Boundary Layers", AGARD Symp. on Fluid Dynamics of Three - Dimensional Turbulent Shear Flows and Transition, Cesme, Turkey, 1988.

10. Spall, R.E. and Malik, M.R., "Effect of Transverse Curvature on the Stability of Compressible Boundary Layers", AIAA J., *29*, 10, 1991, pp 1596 - 1602.

11. Cebeci, T., Chen, H.H. and Kaups, K. "Further Consideration of the Effect of Curvature on the Stability of Three-Dimensional Flows", Computers Fluids, *21*, 4, 1992, pp 491 - 502.

12. Spall, R.E. and Malik, M.R., "Linear Stability of Three - Dimensional Boundary Layers over Axisymmetric Bodies at Incidence", AIAA J., *30*, 4, 1992, pp 905 - 913.

13. Lin, R. - S. and Reed, H.L., "Effect of Curvature on Stationary Crossflow Instability of a Three - Dimensional Boundary Layer", AIAA J., *31*, 9, 1993, pp 1611 - 1617.

14. de Bruin, A.C., "COSALX - A Method for Linear Stability Analysis of Three- Dimensional Compressible Boundary Layers", NLR TR 90130 L, The Netherlands, 1990.

15. Kaups, K. and Cebeci, T., "Compressible Laminar Boundary Layers on Swept and Tapered Wings", J. Aircraft, *14*, 1977, pp 661 - 667.

16. Malik, M.R., "Finite - Difference Solution of the Compressible Stability Eigenvalue Problem", NASA CR 3584, 1982.

17. Seitz, A., "Ermittlung des Querströmungs-N - Faktors zur Umschlagvorhersage im Niedergeschwindigkeitswindkanal Braunschweig", IB 129 - 89/26, DLR Braunschweig, 1989.